Sci

MDPI

Article

Processing and Characterization of AlN–SiC Composites Obtained by Spark Plasma Sintering

Tatiana N. Smetyukhova [1,2,*], Levko Arbanas [2], Anton D. Sokolov [2], Viktoria E. Bazarova [2], Yuri Pristinskiy [1], Anton Smirnov [1] and Nestor Washington Solis Pinargote [1,*]

[1] Spark Plasma Sintering Research Laboratory, Moscow State University of Technology "STANKIN", Vadkovsky per. 1, 127055 Moscow, Russia; a.smirnov@stankin.ru (A.S.)
[2] Laboratory of Ceramic Materials and Technology, MIREA—Russian Technological University, Vernadsky Avenue 78, 119454 Moscow, Russia; laklic@mail.ru (A.D.S.)
* Correspondence: smetyukhova.t.n@yandex.ru (T.N.S.); nw.solis@stankin.ru (N.W.S.P.)

Abstract

In this paper, the dependence of the microstructure and properties on Spark Plasma Sintering modes of an AlN-35 β-SiC (wt.%) composite is investigated. It was found that the use of a heating rate of 100 °C/min during the sintering process of the AlN-35 β-SiC (wt.%) composite leads to the formation of a solid solution $(AlN)_x$–$(SiC)_{x-1}$ at 1900 °C during 5 min, and under a pressure of 50 MPa. It was observed that, at a heating rate of 50 °C/min and a pressure of 25 MPa, yttrium oxide used as a sintering additive impedes the diffusion of SiC into AlN. This impedes the formation of a solid solution $(AlN)_x$–$(SiC)_{x-1}$ and helps preserve SiC grains, which act as the main absorbing phase in the obtained composites. It is shown that the use of sintering additives and SPS technology allows obtaining samples with a density of 3.26 g/cm^3, which coincides with the theoretical value of the composite. The dielectric characteristics and absorbing properties of sintered materials are determined in the frequency bands from 5.6 to 26 GHz. It has been discovered that the reflection, transmission, and absorption coefficients can be regulated depending on the thickness of the sample. In addition, it is shown that composites containing solid solutions and silicon carbide grains in their structures have the best absorbing properties. On the other hand, the material containing only solid solutions is a promising material that can be used as microwave filters.

Keywords: silicon carbide; aluminum nitride; spark plasma sintering; dielectric properties

check for updates

Academic Editor: Masami Okamoto

Received: 19 September 2025
Revised: 10 November 2025
Accepted: 26 November 2025
Published: 1 December 2025

Citation: Smetyukhova, T.N.; Arbanas, L.; Sokolov, A.D.; Bazarova, V.E.; Pristinskiy, Y.; Smirnov, A.; Pinargote, N.W.S. Processing and Characterization of AlN–SiC Composites Obtained by Spark Plasma Sintering. *Sci* **2025**, *7*, 174. https://doi.org/10.3390/sci7040174

Copyright: © 2025 by the authors. Licensee MDPI, Basel, Switzerland. This article is an open access article distributed under the terms and conditions of the Creative Commons Attribution (CC BY) license (https://creativecommons.org/licenses/by/4.0/).

1. Introduction

Silicon carbide (SiC) is a promising ceramic material due to its excellent physicochemical properties, including good mechanical properties at room and high temperatures, high thermal conductivity and hardness, good dielectric properties, and excellent resistance to corrosion and oxidation [1]. Moreover, silicon carbide is a refractory material that has higher strength, hardness, and creep resistance compared to aluminum nitride (AlN). In addition to the excellent mechanical properties and high thermal conductivity of SiC, this material is also an excellent absorber of electromagnetic radiation in the microwave range (300 MHz–300 GHz).

Ceramic composite based on the AlN-SiC system is one of the most promising materials for microwave energy absorption, in which aluminum nitride acts as a heat-dissipating matrix and silicon carbide acts as an energy-absorbing phase. SiC-AlN-based composites

combine the excellent properties of two materials in one ceramic composite, such as high temperature resistance, high thermal conductivity, and various electrical properties, from semiconductor to insulating. Due to the dielectric properties, high temperature resistance, and thermal conductivity of AlN-SiC composites, they are considered suitable materials for high-temperature electronic ceramics. For instance, these composites are widely used in the manufacture of substrates with high thermal conductivity for high-power applications in microcircuits, functional electronics, as well as structural elements that act as microwave radiation absorbers.

Due to the strong covalent bonds of AlN and SiC, it is very difficult to obtain dense materials from them at low sintering temperatures without the use of external pressure or additives that improve sintering. Therefore, different oxides of rare earth elements and metals are often used as sintering additives in the consolidation of AlN and SiC ceramics. Currently, SiC-AlN ceramics are usually produced by hot pressing (HP) and pressureless sintering [2–4].

Lu et al. [5] investigated the effect of SiC particle size on the density and properties of an AlN-SiC composite obtained by free sintering at 2000 °C. Before sintering the powder AlN-SiC mixture with yttrium oxide (Y_2O_3) as the sintering additive was uniaxially pressed and then cold isostatically pressed in order to obtain disk samples that were heated in a nitrogen atmosphere. In this study it was found that SiC particle sizes have a great influence on the properties, and the AlN–SiC composite with a SiC particle size of 2 microns demonstrates the best combination of properties: density—3.292 g/cm^3, thermal conductivity—45.53 W/(m·K), electrical resistance in the order of 10^8 Ω·m, dielectric constant—14–17 and tangent of dielectric loss angle (dielectric loss, tgδ)—0.37–0.47 in the range from 8.2 to 12.4 GHz.

Gu et al. [6] produced SiC-AlN multiphase ceramics by free sintering using Y_2O_3-BaO-SiO_2 as a sintering additive. The cold isostatic pressed samples were sintered at temperatures from 1750 °C to 1900 °C for 1 h in a nitrogen atmosphere. Samples with Y_2O_3 (4–8 wt.%)-BaO (1.12 wt.%)-SiO_2 (0.88 wt.%), and different SiC content (40, 45, 50, 55, 60 wt.%) were fabricated. The results of this study show that, after sintering, a low content of complex oxides $Y_3Al_5O_{12}$ and $Y_4Al_2O_9$ was formed. Moreover, the SiC-AlN ceramics with 50 wt.% SiC and sintered at 1900 °C showed a dielectric loss of 0.4–0.5 and a dielectric constant of 33–37 in the frequency range from 2.4 to 18 GHz, and the highest values of thermal conductivity 61.02 W/(m·K).

In another work, Prikhna et al. [7] have shown that an increase in the SiC content in the AlN-SiC composite leads, on the one hand, to an increase in energy absorption and, on the other hand, to a decrease in mechanical properties due to an increase in porosity. The results of this work confirm that one of the main problems in the production of AlN-SiC composites that needs to be solved is decreasing the porosity of the sintered AlN-SiC composites while maintaining high levels of their operational properties.

It is well known that Al_2O_3, Y_2O_3, CaO, or Er_2O_3 are used as sintering additives for the liquid phase sintering of AlN and SiC [8–10], in which the sintering temperature decreases significantly, the consolidation process accelerates, and a significantly higher density of the composite material is achieved. Moreover, these additives can change the properties of the composites; for instance, the presence of Al_2O_3 in AlN-based ceramics increases their oxidation resistance, mechanical strength, and thermal stability [8]. In addition, the study of Nepochatov et al. [9] shows that the introduction of 3 wt.% Y_2O_3 into an AlN-based mixture led to a significant increase in the thermal conductivity of the composite up to 164 W/(m·K) as a result of the oxygen removal from the aluminum nitride lattice and due to the formation of yttrium aluminium garnet ($Y_3Al_5O_{12}$). On the other hand, the addition of AlN-Er_2O_3 in an amount of 10 vol.% to SiC pow-

der significantly increases the strength of the composite sintered at temperatures from 1600 °C to 550 MPa, due to the formation of a refractive grain-boundary glassy phase [10].

Improving the mechanical properties of AlN-SiC composites can be achieved by creating their joint solid solution. Due to the similar crystal structure and high-temperature properties of both SiC and AlN, the $(SiC)_x(AlN)_{1-x}$ solid solutions have unique mechanical properties, such as the formation of homogeneous solid solutions leads to increased bending strength and crack resistance [11]. In addition, owing to the formation of AlN-SiC solid solutions, sintering activity, microstructure, mechanical and functional properties, as well as oxidation resistance of the composite are significantly improved. For instance, Shirouzu et al. [12] indicated that the excellent crystall cell compatibility of 2H-SiC and 2H-AlN makes it possible to obtain a complete solid solution in a wide compositional range (SiC/10–90 mol% AlN) under certain conditions (above 1900 °C).

Safaraliyev et al. [13] studied the dielectric constant and the dielectric loss in polycrystalline solid solutions $(SiC)_x(AlN)_{1-x}$ depending on the component content and frequency. It was found that at concentrations from 30 to 50 wt.% SiC abnormally high values of the dielectric constant and the tangent of the dielectric loss angle at low frequencies (0.1 kHz) are observed in AlN. Moreover, it was shown that an increase in the dielectric constant can be associated with the barrier effect at the grain boundaries of silicon carbide and aluminum nitride, as well as with migration polarization.

As is well known, there are four polarisation modes in a dielectric medium, including electron polarisation (10^{14}–10^{18} Hz), ion polarisation (10^{12}–10^{14} Hz), dipole polarisation (10^{8}–10^{10} Hz), and space charge polarisation (10^{0}–10^{4} Hz). The dominant polarisation modes in AlN–SiC composites are electron and dipole polarisation. The loss peak is related to withdrawal and transformation of electron polarisation as well as dipole polarisation; in addition, the high concentration of dipole polarisation would be an impact factor of shifts to low-frequency [14,15].

In the work of Xiang-Yu et al. [2], ceramics based on SiC-AlN solid solutions were obtained by HP at 2200 °C in argon under a pressure of 40 MPa for 90 min. In the samples, the amount of SiC varied in the range of 10–80 wt.%, and a small amount of boron was also added as the sintering additive, which made it possible to obtain dense sintered samples of SiC-AlN composites. These composites consisted of heterogeneous solid solutions of $(SiC)_x(AlN)_{1-x}$ and boron nitride. The formation of heterogeneous solid solutions for samples with an AlN content of less than 20 wt.% is consistent with the work [16]. The sample with 10 wt.% AlN shows the highest dielectric constant and the dielectric loss in the range from 8.5 to 12.5 GHz.

In another work, Fang et al. [3] obtained high-density SiC-AlN composites by HP at 1900 °C in nitrogen under 25 MPa for 90 min. In the samples, the amount of β-SiC varied in the range of 5–40 vol.%, and a complex sintering additive of oxides (4% Y_2O_3 + 2% Al_2O_3) was used. X-ray diffraction showed the presence of a solid solution that promotes the sintering process and also improves the dielectric properties of the composite formed at the interface of the SiC and AlN phases. The presence of β-SiC slows down the AlN grains' growth and leads to the formation of a SiC-AlN solid solution during sintering. As the β-SiC content increases to 40 vol.%, the conductivity of the composites monotonously increases and demonstrates typical percolation behavior at 17.5 vol.%. The sample with 25 vol.% β-SiC shows optimal microwave absorption performance with four peaks in the X-band (8–12 GHz) at 3.5–5 mm thicknesses. As shown in this work, the absorption performance in terms of optimal frequency and thickness is significantly tunable for 25–40 vol.% β-SiC samples.

Despite the advantages of HP, this method is characterized by high cost due to long sintering cycles at high temperatures, which contributes to uncontrolled grain growth. In

the last decades, Spark Plasma Sintering (SPS) has been commonly used as the method for the consolidation of difficult-to-sinter materials and composites [17,18]. The advantage of this technique lies in the high speed of heating and cooling, enabling a reduction in processing time. This avoids unwanted grain growth in the sintered material and improves its properties [19].

The obtention of AlN-SiC ceramics by SPS has been poorly studied, as evidenced by the small number of works [11,12,20–24]. In most of these papers, the authors mainly studied the effect of the powder particle size on the microstructure and mechanical properties of ceramics, and not the dielectric properties and the ability to absorb electromagnetic radiation. The analysis of these works showed that the microstructure of sintered AlN-SiC composites depends on the sintering parameters and particle size of the SiC and AlN raw powders. Microstructure can consist either of individual grains of AlN and SiC [12,22] or of solid solutions $(SiC)_x(AlN)_{1-x}$ [11,12,20,21,23,24].

On the other hand, Gao et al. [11] studied the dielectric properties of AlN/SiC composites obtained by SPS. Here, AlN (d50 = 2 μm) and SiC (d50 = 40 nm) raw powders were used for the preparation of mixtures, in which the SiC content varied between 20 wt.% and 40 wt.%. AlN and SiC powders were mixed with absolute ethanol as a dispersant by high-energy ball milling for 20 min. The powder mixtures were then sintered by SPS in vacuum at 1600 °C, under 30 MPa, for 5 min with a heating and cooling rate of 100 °C/min. X-ray diffraction analysis showed that the sintered samples consisted of β-SiC, AlN, 2H-SiC, and Fe5Si3, the latter being obtained by the reaction of Si with Fe atoms that were introduced into the AlN-SiC composite as a result of wear of the steel grinding balls and pot. The sample relative density was varied from 91.4% to 94.8% as the SiC content decreased. Dielectric constant and dielectric losses measurements on the AlN-35 wt.% SiC composite show a slight increase between 12.4 and 18 GHz, unlike other compositions, which makes this composition a promising broadband microwave absorber in the studied frequency range. The dielectric losses for AlN-35 wt.% SiC composite were more than 0.48, and the dielectric constant was about 20.

The effect of sintering additives on the structure and dielectric properties of AlN/SiC ceramics obtained by SPS was not studied in detail [20]. However, Serbenyuk et al. [4] studied the influence of SiC particle size and the use of Y_2O_3 as a sintering aid on the structure and properties of AlN-SiC composites obtained by pressureless sintering in a nitrogen atmosphere at 1900 °C in a vacuum furnace. This study showed that, during sintering, thin layers of $Y_3Al_5O_{12}$ were formed at the interfacial boundaries between the AlN matrix and SiC grains. Moreover, it was found that the $Y_3Al_5O_{12}$ phase acts as an obstacle to the formation of AlN-SiC solid solutions. Furthermore, it was observed that the electrical resistivity of the compound decreases from 10^4 to 90 Ω·m. when the average size of the SiC inclusions is from around 3 to 7 microns. The decrease in resistivity was explained by the insufficient formation of $Y_3Al_5O_{12}$ at the boundaries of SiC inclusions with a size around 5–7 microns, which intensifies the diffusion processes towards the formation of $(AlN)_x$–$(SiC)_{x-1}$ solid solutions. At the same time, Serbenyuk et al. showed that the absorption of the composite decreases from 37 to 27 dB/cm, while the porosity increases from 1–2% to 7%. This high porosity prevents the use of these compounds as microwave radiation absorbers, since during operation of the device at high temperatures (~800 °C), some elements can escape from the porous material, settle on the cathode, and hinder its operation. Porosity of no more than 5% ensures the effective operation of this composition as an absorbent material, ensuring reliable operation of devices.

The aim of this work is to study the influence of the Spark Plasma Sintering Modes on the structure, dielectric, and absorption properties of an AlN-35 SiC wt.% composite with the use of Y_2O_3 as sintering aid. The choice of the AlN-35 SiC wt.% system is related to the

results obtained in the work [11], which qualify this composition as a promising broadband microwave absorber. For this purpose, it is proposed to study the phase composition and elemental distribution of composites obtained under different sintering modes by SPS. In addition, it is proposed to study the dielectric and absorption properties in a wide frequency range (from 5.6 GHz to 26 GHz).

2. Materials and Methods

2.1. Powder Processing and Sintering

Commercially available AlN + 3 wt.% Y_2O_3 and β-SiC (ТУ 88-1-84-91) were obtained from Merzhanov Institute of Structural Macrokinetics and Materials Science "ISMAN", (Chernogolovka, Russia) as raw materials. The elemental analysis of the raw powders was provided by the manufacturer, and it is shown in Table 1.

Table 1. Chemical composition of the starting powders in wt.%.

Powder	N	O	Fe	C	Si	Al	Y	Free Si	Free C
AlN + 3 wt.% Y_2O_3	32.01	1.62	0.09	0.04	0.07	63.81	2.36	-	-
β-SiC	-	1.33	0.05	28.55	69.4	-	-	0.42	0.25

The theoretical content of each phase by mass and volume fraction of the AlN-35 β-SiC wt.% is shown in Table 2.

Table 2. Phase content in AlN-35 β-SiC composites.

	AlN	β-SiC	Y_2O_3	Theor. Density
wt.%	63.05	35.00	1.95	3.26
vol.%	63.14	35.59	1.27	

The mean particle sizes of AlN and β-SiC were 2.4 and 1.6 μm, respectively. The initial powders were mechanically mixed in a ball mill with SiC balls (∅3 mm) in an Isopropanol medium. Figure 1 shows the elemental distribution maps of powder mixture after mixing determined by EDS, which are denoted within the micrographs with the respective elements: aluminum (Al), silicon (Si), carbon (C), nitrogen (N), oxygen (O), and yttrium (Y).

The obtained AlN-35 β-SiC wt.% wet mixture was dried at 70 °C for 12 h in a vacuum, and the dry mixture was sieved through a 100 μm sieve. Then, the powder mixture was sintered in a H-HP D 25 SD Spark Plasma Sintering machine (FCT Systeme GmbH, Rauenstein, Germany) in vacuum according to the sintering modes presented in Table 3. The produced samples had a diameter of 41 mm and a height of 2.7–2.9 mm.

Table 3. Sintering conditions of SiC-AlN composites.

Sample Number	Sintering Temperature, °C	Pressure, MPa	Isothermal Time, min	Heating Rate up to 1800 °C, °C/min	Heating Rate from 1800 °C to 1900 °C, °C/min
SPS 1521	1900	25	5	50	25
SPS 1522	1900	50	5	50	25
SPS 1523	1900	50	5	100	25

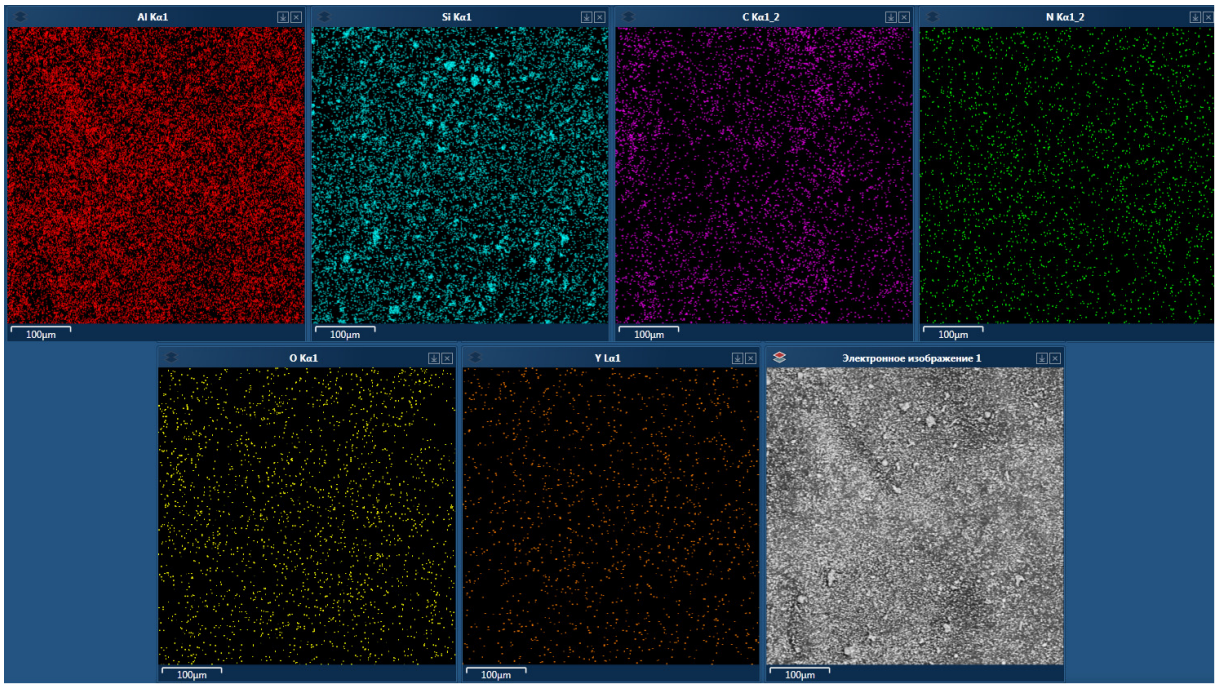

Figure 1. Elemental distribution maps of aluminum (Al), silicon (Si), carbon (C), nitrogen (N), oxygen (O), and yttrium (Y) of the powder mixture after mixing, as well as the SEM image of this mixture.

2.2. X-Ray Diffraction (XRD), Density, Hardness, and Microstructure Characterization

The sintered samples were polished using diamond polishing slurries with grit sizes ranging from 9 µm to one micrometer. After polishing, the samples were washed in an ultrasound bath in ethanol for 15 min and dried using compressed air. The phase composition was characterized by X-ray diffraction (XRD), on a PowDIX600 X-ray diffractometer (LINEV ADANI, Minsk, Belarus) with CuKα radiation, software Search-Match 3 and PDF-2 database.

Bulk densities of sintered samples were determined using the Archimedes method in distilled water. For this, before measurement, the samples were dried in a vacuum drying oven at 120 °C for 2 h until a constant weight was reached. After drying, the mass of the samples in air was measured (m_1) using an AND GR-200 balance (A&D, Tokyo, Japan). Next, the samples were saturated with water using a vacuum system consisting of a vessel and a vacuum pump. For saturation, the samples were immersed in a beaker filled with water, and then the beaker was placed in the vacuum system. A pressure of 400 mbar was then created in the vacuum system at room temperature, and the samples were kept under these conditions for 1 h. After this time, the mass of the saturated samples was determined (m_2) in air. Then, the mass of the saturated sample immersed in water was determined (m_3) using the density determination kit AD-1653 (A&D Company, Tokyo, Japan).

The bulk density (ρ) in g/cm^3 was calculated using the following Formula (1):

$$\rho = \frac{m_1}{m_2 - m_3} \cdot \rho_l, \quad (1)$$

where m_1 is the mass of the dry sample [g]; m_2 is the mass of the sample saturated with water [g]; m_3 is the mass of the saturated sample immersed in distilled water [g]; ρ_l is the density of water at the test temperature, g/cm^3.

Water absorption (W) was calculated using the following Formula (2):

$$W = \frac{m_2 - m_1}{m_1} \cdot 100\%. \quad (2)$$

Open porosity (OP) was calculated using the following Formula (3):

$$OP = \frac{m_2 - m_1}{m_2 - m_3} \cdot 100\%. \quad (3)$$

The theoretical density of the AlN-35 β-SiC wt.% composite was calculated using AlN, SiC, and Y_2O_3 densities of 3.26, 3.21, and 5.01 g/cm^3, respectively. The relative density of the samples was then calculated as the bulk density divided by the theoretical density and multiplied by 100%.

The polished and fractured surfaces of the samples were observed by scanning electron microscopy (SEM) VEGA 3 LMH(Tescan, Brno, Czech Republic) equipped with an energy dispersive spectroscopy (EDS) detector X-Act EDX (Oxford Instruments, Abingdon, UK).

Vickers hardness (Hv) was measured by the indentation method using a universal microhardness tester (Qness, Salzburg, Austria) with a standard diamond pyramid indenter, using a load of 19.6 N during 10 s. A minimum of 10 indentations was made, and then the arithmetic mean of the test results for each composition was calculated. The hardness was calculated by the equation $HV = 0.1891\ P/d^2$, where P is the load (N), and d is the average length of two diagonals (mm).

2.3. Dielectric, Electrical, and Microwave Absorption Properties

The transmission coefficient of electromagnetic energy through a disk sample (∅ = 41 mm; h = 2.5 and 2 mm) was measured in the frequency range of 5.64–8.24 GHz using the waveguide technique by the scalar network analyzer (frequency-sweep generator Ya2R-75 and frequency indicator Ya2R-70, Russia) and the transmission line with the rectangular waveguide of a section 35 × 15 mm^2. The 2 mm high disk samples were obtained after grinding the 2.5 mm high samples.

Furthermore, the microwave absorption characteristics (reflection and transmission coefficients), dielectric constant and loss tangent, in the frequency range of 8–12 GHz (X-band), 12–18 GHz (P-band) and 18–26 GHz (K-band), were measured by the waveguide method Nicolson–Ross–Weir [25,26] using a network analyzer Agilent E8363B (Agilent Technologies, Santa Clara, CA, USA). Depending on the frequency range studied, parallelepipeds with different dimensions were cut from disk samples: X-Band (22.9 × 10.1 × 2.0 mm^3), P-Band (15.7 × 7.9 × 2.0 mm^3), K-Band (10.6 × 4.2 × 2.0 mm^3). After the first series of measurements, the samples were ground to a height of 1 mm to measure their characteristics.t The absorption coefficient (A) was calculated by the following:

$$\begin{aligned} A &= 1 - T - R, \\ T &= 10^{Tc/10}, \\ R &= 10^{Rc/10}, \end{aligned} \quad (4)$$

where T is the transmission coefficient, Tc is the transmission coefficient in dB, R is the reflection coefficient, and Rc is the reflection coefficient in dB.

In addition, the capacitance, loss tangent, and resistivity of samples (10.6 × 4.2 × 1.0 mm^3) were measured at a frequency of 1 MHz using a GW Instek LRC-

meter (Good Will Instrument Co., Ltd., Xinbei, Taiwan). For these samples, the dielectric constant (ε) was calculated by the following:

$$\varepsilon = \frac{C_p \cdot h}{\varepsilon_0 \cdot S}, \quad (5)$$

where C_p is capacitance (F), h is the thickness of the sample (m), ε_0 is the permittivity of vacuum (8.854×10^{-12} F/m), and S is the surface area of the electrode of the sample (m^2).

The electrical resistance ($\Omega \cdot m$) was calculated by the following:

$$\rho_V = \frac{R_v \cdot S}{h} \quad (6)$$

where R_V is resistivity (Ω), h is the thickness of the sample (m), and S is the surface area of the electrode of the sample (m^2).

3. Results and Discussion

3.1. Density, Phase Compositions, and Microstructure

The values of density, open porosity, water absorption, and Vickers Hardness of sintered samples are given in Table 4.

Table 4. Density, open porosity, and hardness of sintered SiC-AlN composites.

Sample Number	W *, %	OP *, %	ρ *, g/cm^3	ρ_{rel} *, %	HV *, GPa
SPS 1521	0.07	0.23	3.224 ± 0.003	98.77	17.8 ± 1.7
SPS 1522	0.02	0.06	3.256 ± 0.003	100	18.2 ± 1.2
SPS 1523	0.01	0.03	3.257 ± 0.003	100	17.5 ± 0.7

*: W—Water absorption; OP—Open porosity; ρ—Density; ρ_{rel}—Relative density; HV—Vickers Hardness.

From Table 4, it is observed that the density of the sintered samples reached the theoretical value. Moreover, the results related to water absorption and open porosity confirm that the use of Y_2O_3 as the sintering aid and selected technological sintering modes reduces the amount of pores in the sintered samples.

The XRD patterns of the sintered samples SPS 1521- SPS 1523 are shown in Figure 2. In this figure it can be observed that the peaks corresponding to phase AlN (2H, PDF 79-2497), solid solutions 4H SiC (PDF 29-1127) and 2H SiC (PDF 29-1126) are observed on all diffractograms, while the peaks corresponding to the β-SiC phase (3C SiC, PDF 29-1129) are observed only in the samples SPS 1521 and SPS 1522.

The quantitative phase ratio is difficult to determine due to the superposition of diffraction peaks of different phases on top of each other. From the obtained results, it can be assumed that sample SPS 1523 consists of solid solutions $(SiC)_x(AlN)_{1-x}$ and aluminum nitride, while samples SPS 1521 and SPS 1522 contain more β-SiC (3C) grains.

Figure 3 shows the surfaces' SEM images of composites SPS 1521, SPS 1522, and SPS 1523. Figure 3a,b shows that samples 1521 and 1522 have a heterogeneous microstructure with large agglomerates, presumably consisting of silicon carbide. However, these agglomerations are absent in sample SPS 1523 (Figure 3c). For a more detailed study of the distribution of SiC grains in the AlN matrix, EDS analysis of the samples was performed.

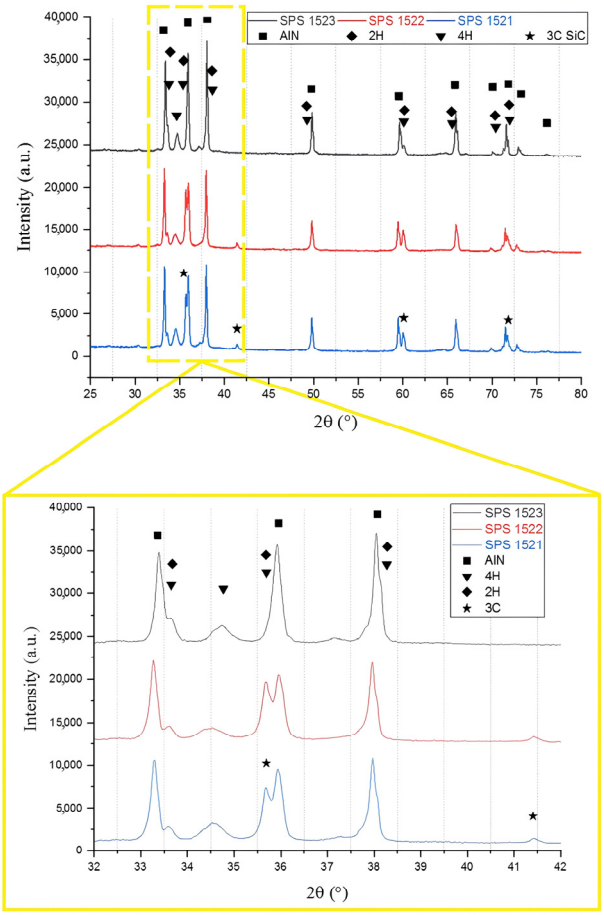

Figure 2. XRD analysis of sintered 1521–1523 samples. Enlargement section of the diffractogram from 32° to 42° of 2Theta.

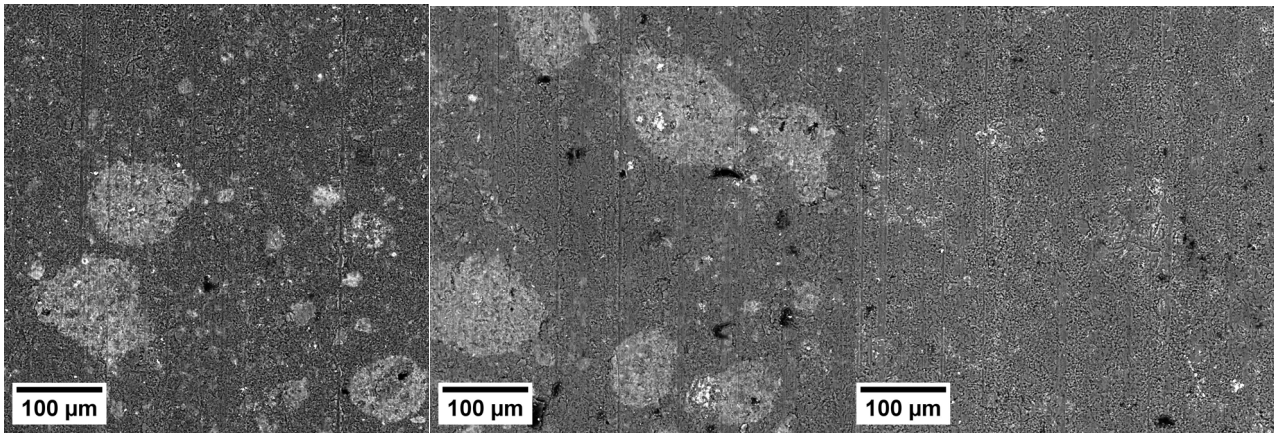

(**a**) (**b**) (**c**)

Figure 3. Surfaces' SEM images of sintered composites SPS 1521 (**a**), SPS 1522 (**b**), and SPS 1523 (**c**).

Figures 4–6 show the elemental distribution maps determined by EDS, which are denoted within the micrographs with the respective elements: aluminum (Al), silicon (Si), yttrium (Y), carbon (C), oxygen (O), and nitrogen (N).

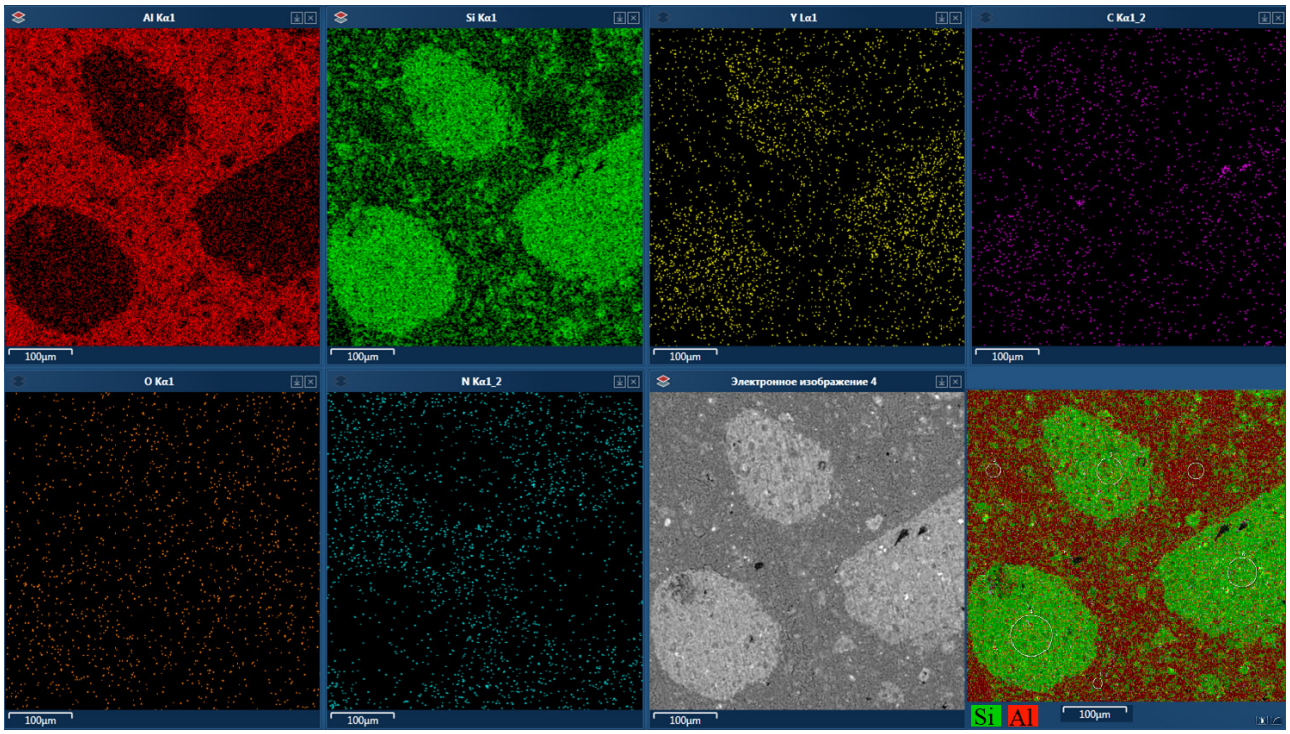

Figure 4. Elemental distribution maps of aluminum (Al), silicon (Si), yttrium (Y), carbon (C), oxygen (O), and nitrogen (N) on the sample surface SPS 1521, as well as the surface SEM image, and the combination of Si and Al maps.

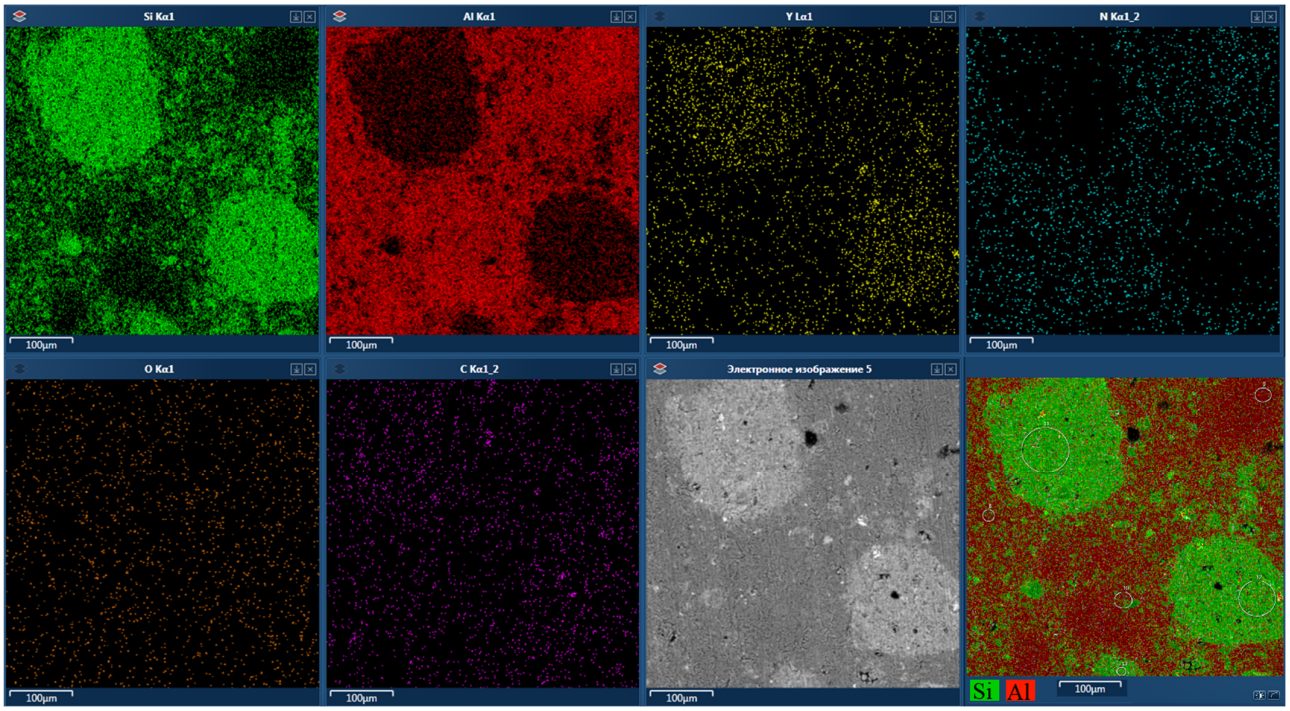

Figure 5. Elemental distribution maps of silicon (Si), aluminum (Al), yttrium (Y), nitrogen (N), oxygen (O), and carbon (C) on the sample surface SPS 1522, as well as the surface SEM image, and the combination of Si and Al maps.

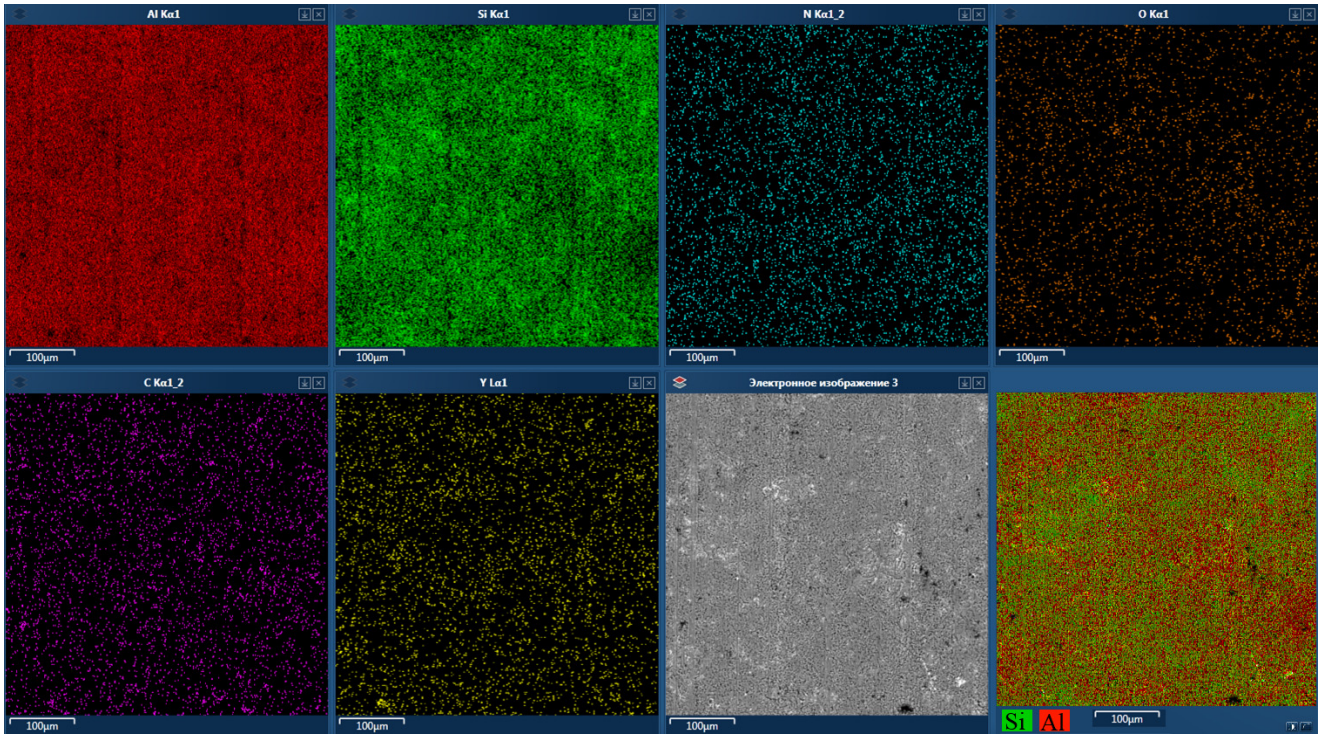

Figure 6. Elemental distribution maps of aluminum (Al), silicon (Si), nitrogen (N), oxygen (O), carbon (C), and yttrium (Y) on the sample surface SPS 1523, as well as the surface SEM image, and the combination of Si and Al maps.

From the obtained distribution maps, it can be concluded that the microstructure of the samples SPS 1521 and SPS 1522 is heterogeneous, and the SiC grains are preserved inside the AlN matrix. On the other hand, the element distribution of the SPS 1523 sample surface demonstrates a characteristic pattern for a solid solution: a uniform distribution of all elements in the area under study, as well as the absence of areas corresponding to silicon carbide grains (Figure 6).

From this analysis it can be concluded that the SPS of the AlN-35 β-SiC wt.% mixture under a pressure of 25 MPa and a combination of heating rates of 50 °C/min (from 300 to 1800 °C) and 25 °C/min (from 1800 to 1900 °C) with an dwell time of 5 min at 1900 °C (Table 3, SPS 1521 sample) produces samples with a relative density of 98.77% and a heterogeneous structure of SiC grains in the AlN matrix (Figure 4).

On the other hand, only the variation of one of the sintering conditions, namely, the increase in the pressure up to 50 MPa (Table 3, SPS 1522 sample), allows the obtaining of samples with a relative density of 100%, but with a heterogeneous structure similar to that explained above (Figure 5). A further variation of the sintering conditions, namely, increasing the heating rate from 50 °C/min to 100 °C/min (Table 3, SPS 1523 sample), allows the obtaining of samples with a relative density of 100%, but with a structure of a solid $(SiC)_x(AlN)_{1-x}$ solution, in which the SiC particles become dissolved in the sample matrix, and a fairly uniform distribution of aluminum and silicon throughout the volume is observed (Figure 6). These results are fully in agreement with the XRD patterns in Figure 2 and confirm the assumption made earlier about the structures of the sintered samples.

As is known, the consolidation of materials at high speeds by SPS is driven by different phenomena, namely, plasma generation, Joule heating, pulsed current, and mechanical pressure [27]. Olevsky et al. [28] divide these phenomena into two groups: those of a thermal and those of a nonthermal nature. These authors explain that, during SPS, the phenomena of the first group produce extremely high heating rates, which impact vacancy

concentrations, creating, in a short time, the conditions necessary for local melting in the contact areas between particles and generating thermal stresses that stimulate dislocation creep. This, in turn, accelerates diffusion and densification rates during SPS sintering. The second group is related to the direct influence of the electromagnetic field on mass transport by diffusion through electromigration, the "throttling" effect, electroplasticity mechanisms, ponderomotive forces, and dielectric breakdown of oxide films, including the cleaning effect and the generation of defects at grain boundaries. Thus, it can be concluded that the use of high heating speeds, thanks to the combined action of the aforementioned phenomena, leads to a rapid diffusion of the material, even ceramic material.

In previous works [29,30], hypotheses were proposed stating that SiC particles dissolve and Si and C atoms diffuse into AlN to form a solid solution. For example, the SPS of a powder containing 90SiC-10(AlN + Y_2O_3) (mol%) under 30 MPa, 100 °C/min, 1900 °C, and a dwell time of 10 min produced composites containing only SiC grains and a 2H solid solution in the intergranular space, formed by the diffusion of SiC into the AlN [31].

In our study, when applying a heating rate of 100 °C/min during SPS of the AlN-35 β-SiC wt.% mixture, accelerated diffusion occurred, thus accelerating the solid solution formation process. However, the structure obtained in the sample SPS 1523 contained two solid solutions, 2H and 4H. It can be assumed that obtaining a single solid solution 2H from this mixture requires a dwell time greater than 5 min, since the 5 min used proved insufficient to complete the mass transport by diffusion process.

Applying a heating rate of 50 °C/min (up to 1800 °C) corresponds to a diffusion rate of SiC in AlN lower than that obtained at 100 °C/min. As can be seen in the obtained results (Figures 2–5), a low diffusion rate combined with a holding time of 5 min is insufficient to achieve the intensive dissolution of SiC in AlN and the formation of a completely solid solution, as occurs, for example, during hot pressing [29].

From Figures 4 and 5, it is worth noting that the yttrium distribution maps coincide with the silicon maps for each of the samples examined (SPS 1521 and SPS 1522). Based on this, it can be assumed that in these samples yttrium oxide prevents the diffusion of aluminum nitride into silicon carbide, i.e., the formation of a solid solution $(SiC)_x(AlN)_{1-x}$, and promotes the preservation of silicon carbide grains with a 3C structure. A similar phenomenon was observed in work [4], where it is assumed that a $Y_3Al_5O_{12}$ phase is formed during sintering as thin layers at the interfacial boundaries between the matrix phase of AlN and SiC grains. In the AlN-SiC composite, the phase $Y_3Al_5O_{12}$ can act as an obstacle to the formation of AlN-SiC solid solutions. In our case, the absence of intense peaks on diffractograms corresponding to any crystal structure containing yttrium atoms indicates its uniform distribution and dissolution in solid solutions $(SiC)_x(AlN)_{1-x}$ or the formation of very thin interfacial layers at the boundary of the matrix phase and SiC grains, which are undetectable by the X-ray method using this model of diffractometer.

It remains interesting to study the mechanism for the formation of the observed large silicon carbide agglomerates (Figures 3–5) during sintering of the SiC-AlN system by SPS. Similar formation of SiC agglomerates in the SiC-AlN system was already noted in the work of Shirouzu et al. [12]. The authors used SiC (0.3 μm) and AlN (1.1 μm) starting powders, and, after their co-sintering, SiC agglomerates measuring 10–50 μm formed in the composite. However, the authors do not provide a hypothesis regarding the formation mechanism of these agglomerates.

Based on the results obtained in our study, we can assume that the formation of SiC agglomerates may be related to nonuniform heating of the sample [32], caused by the passage of electric current through the material during SPS. It is likely that under the sintering conditions studied, regions with localized high temperature arise where more active dissolution (evaporation or melting) of AlN occurs, promoting the agglomeration and

sintering of SiC instead of its diffusion into AlN [33]. However, when using a heating rate of 100 °C/min, various phenomena occur within the bulk of the material, predominantly the diffusion of SiC particles into AlN. The above description can serve as a preliminary explanation for the observed results.

3.2. Microwave Absorption, Dielectric and Electrical Properties

The transmission coefficient was measured on ground disks, manufactured from samples SPS 1521, SPS 1522, and SPS 1523. The measurements were carried out using the waveguide technique by the scalar network analyzer at frequencies 5.64, 6.00, 6.50, 7.00, 7.50, 7.70, 8.00, and 8.24 GHz. Figure 7 shows the dependence of the transmission coefficient for disk samples with heights of 2.5 and 2.0 mm. From this figure, it can be seen that the sample's thickness significantly affects the transmission coefficient of electromagnetic energy as it passes through it. Figure 7 shows that, for SPS 1523 samples, the highest transmission coefficient is 15 dB at 7.5 GHz. However, as the thickness decreases from 2.5 mm to 2.0 mm, the transmission coefficient decreases from 15 dB to 8.5 dB, respectively. This is consistent with the fact that the thickness of the sample directly influences the transmission coefficient [34]. On the other hand, the highest transmission coefficient for the SPS 1522 sample with a thickness of 2.5 mm is 16.5 dB at 6.0 GHz. As with the sample SPS 1523, the transmission coefficient of the SPS 1522 sample decreases to 15.5 dB when its thickness is reduced to 2.0 mm. The difference in the transmission coefficient for samples SPS 1523 and SPS 1522 is due to the fact that they have different structures after sintering: SPS 1523 has a solid solution $(SiC)_x(AlN)_{1-x}$ (2H and 4H) and aluminum nitride, and SPS 1522 is a composite with SiC inclusions in aluminum nitride. This is in concordance with the fact that the structure and phase composition of the material also influence the transmission coefficient [35].

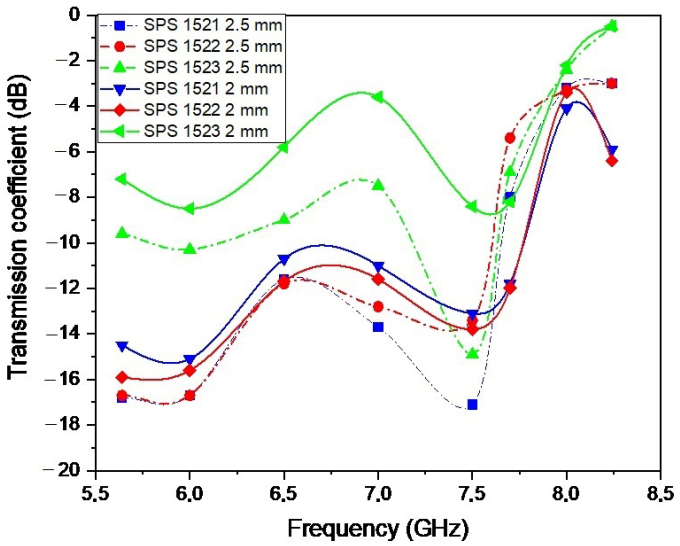

Figure 7. Dependences of the transmission coefficient of sintered 35% SiC-AlN samples at a thickness of 2.0 mm (solid line) and 2.5 mm (dotted line).

The behavior of samples SPS 1521 differs from that previously considered. For instance, sample SPS 1521 with a sample thickness of 2.5 mm shows the highest transmission coefficient (17 dB at 7.5 GHz) among all measurements. However, as its thickness decreases to 2.0 mm, the transmission coefficient at 7.5 GHz decreases from 17 dB to 13 dB, and the highest transmission coefficient of 15 dB is observed at a frequency of 6.0 GHz. This can be related to the fact that samples SPS 1521 are not completely dense (relative density 98.77%), and their structure has pores, in which scattering and absorption of electromagnetic energy

of microwaves occur. This explains its highest transmission coefficient value compared to the completely dense samples SPS 1522 and SPS 1523 (relative density near 100%). As the thickness of the SPS 1521 sample decreases, the number of pores also decreases. With a thickness of 2 mm, the microstructure of the sample has the greatest influence on the transmission coefficient, more than its thickness. The phase composition and microstructure of SPS 1522 and SPS 1521 samples are similar according to X-ray diffraction (XRD) and scanning electron microscopy (SEM). For this reason, the transmission coefficient curves of these two samples with a thickness of 2 mm are almost identical (see Figure 7), also indicating their similarity in phase composition and microstructure.

Using the scalar network analyzer does not allow a detailed study of the effect of sample thickness on their microwave absorption, dielectric, and electrical properties. Therefore, further studies on these characteristics were performed using a network analyzer Agilent E8363B in the frequency range of 8–12 GHz (X-band), 12–18 GHz (P-band), and 18–26 GHz (K-band). Thus, further measurements of reflection, absorption, and transmission coefficients were carried out on parallelepipeds with different dimensions using the Nicolson–Ross–Weir (NRW) method. After the first series of measurements, the samples' thickness was reduced from 2 mm to 1 mm by grinding.

Figure 8 shows the measured values of the reflection and transmission coefficients in the frequency bands 8–12 GHz, 12–18 GHz, and 18–26 GHz. It can be seen from the obtained graphs that the sample sintering mode significantly affects its properties. The rate of heating during sintering, rather than the applied pressure, has the greatest effect on the absorbing properties of the sample material. Analyzing the dependences in Figure 8 of the reflection and transmission coefficients, it can be concluded that the obtained composite ceramic materials consisting of an aluminum nitride matrix, solid solutions and grains of β-SiC silicon carbide (sample SPS 1521 and SPS 1522) have the highest transmission coefficient and absorption of microwave energy: for a sample thickness of 2 mm, transmission is of the order of 14–22 dB in the frequency range of 18–23 GHz, for a sample thickness of 1 mm attenuation of the order of 12–14 dB occurs at a frequency of 8–14 GHz.

Sample SPS 1523, which is 2 mm thick and consists of a solid solution and aluminum nitride, has the lowest reflection coefficient of 8–22 dB in the 22–26 GHz range and the minimum absorption coefficient, making this material a promising material for use as microwave filters.

The differences in the dielectric properties of the samples can be explained by the presence of isolated SiC particles, their size and quantity, as well as the presence of two phases of the solid solution (4H SiC and 2H SiC). For example, Li et al. [15] explain the increase in the tangent of the loss angle by energy dissipation at the grain boundaries of AlN. Furthermore, the authors clarify that the changes in dielectric properties are related to the two states that the SiC grains have in the AlN matrix: (1) SiC exists as the second phase at the grain boundary of AlN; (2) SiC diffuses as Si and C atoms into the lattice of AlN and exists as AlN–SiC solid solutions. In addition, it was found that the energy losses of electromagnetic waves increase due to the increase in scattering occurring at grain boundaries during their propagation in AlN-SiC composites.

A decrease in the thickness of the samples leads to a shift of the minima of the reflection, transmission, and absorption coefficients towards high frequencies, which makes it possible to adjust the absorbing properties of the material by changing its thickness. Figure 9a,b shows the dependences of the dielectric constant and the tangent of the dielectric loss angle of samples in the range of 8–18 GHz, obtained by the NRW method. Due to the resonance occurring in the system under study, it was not possible to determine the values of the dielectric constant and the tangent of the dielectric loss angle for these materials at frequencies above 18 GHz.

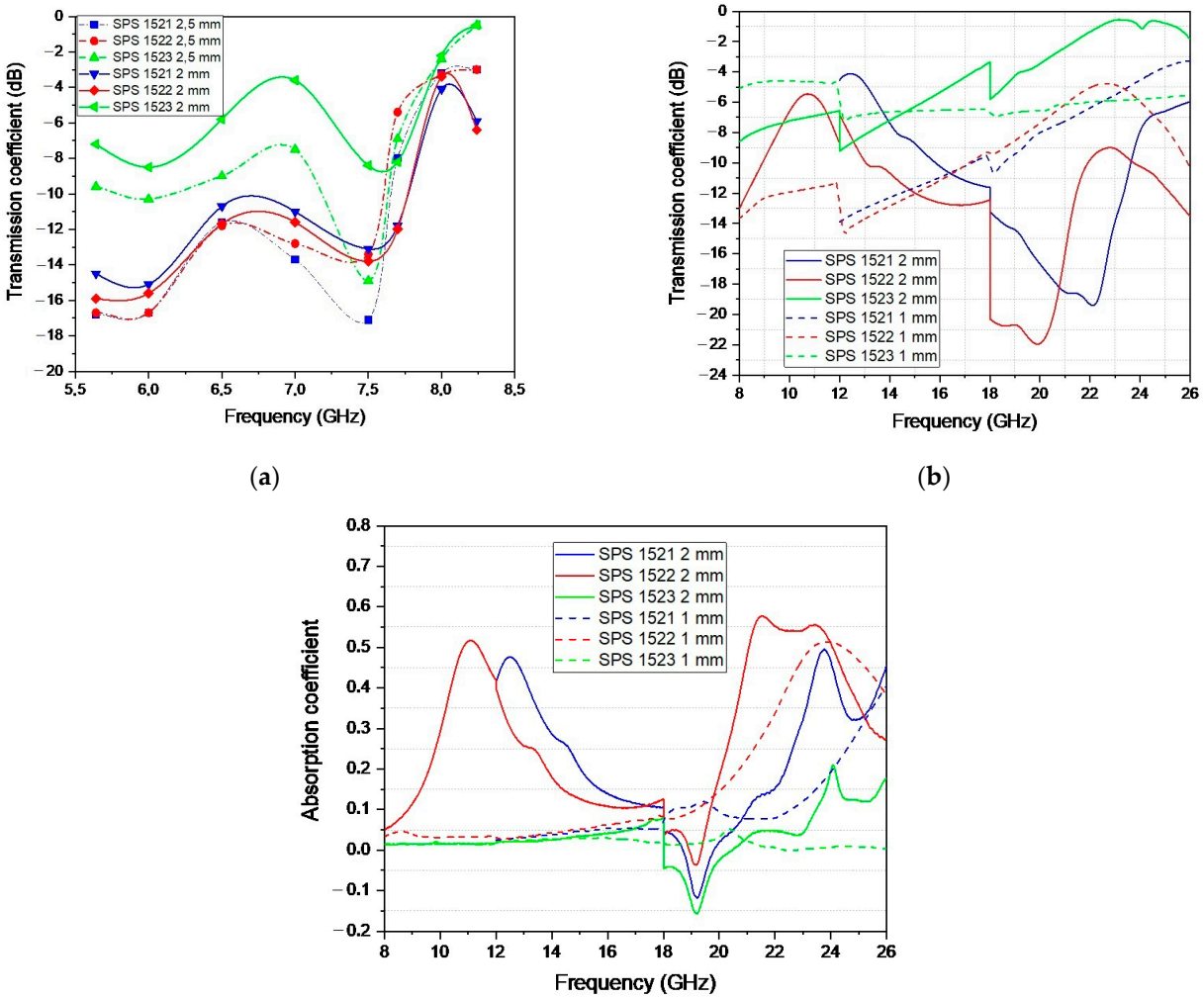

Figure 8. Dependence of (**a**) reflection, (**b**) transmission, and (**c**) absorption coefficients on frequency determined by the NRW method from samples SPS 1521- SPS 1523.

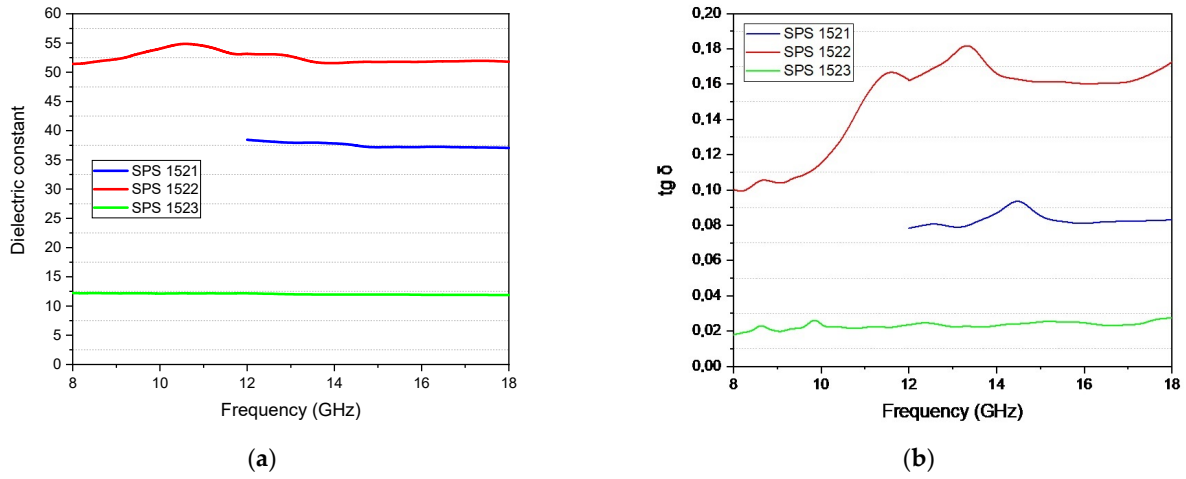

Figure 9. Dependence of (**a**) dielectric constant, and (**b**) dielectric loss tangent on frequency (8–18 GHz) determined by the NRW method from samples SPS 1521- SPS 1523.

A control measurement of the electrical and dielectric properties of the sintered SiC-AlN composites was performed at a frequency of 1 MHz. The results of this measurement are given in Table 5.

Table 5. Electrical and dielectric properties of SiC-AlN composites at 1 MHz.

Sample Number	Capacitance, pF	Dielectric Constant	Loss Tangent	Resistivity, Ω·cm
SPS 1521	20	52	0.700	4.9×10^4
SPS 1522	31	79	1.730	1.3×10^4
SPS 1523	6.5	17	0.002	3.5×10^7

The increase in electrical resistivity of SiC–AlN ceramic from ~10^4 to ~10^7 Ω·cm is presumably due to the formation of solid solutions $(SiC)_x(AlN)_{1-x}$ (2H) via the dissolution of SiC into AlN. This is consistent with the assumptions made in [29,36] that silicon carbide dissolves in aluminum nitride and forms a SiC–AlN solid solution.

In addition, it is observed that the electrical resistivity of SiC–AlN ceramic depends on the sintering method, the SiC raw powder size, and the phase composition of the sintered ceramics. For example, the electrical resistivity of SiC–AlN ceramics obtained by different methods was in the order of 10^1–10^{18} Ω·cm, as shown in Table 6.

The achievement of high values of electrical resistivity presented in Table 6 is explained by the formation of solid solutions, and the addition of large amounts of Y_2O_3, which formed significant quantities of highly insulating Y–Al–Si–O–C–N glass phases in SiC–AlN ceramics [29]. Low values of electrical resistivity can be explained by the high content of semiconductor SiC, which forms a conductive framework in SiC–AlN composites.

Table 6. Electrical resistivity of sintered SiC-AlN composites by different methods.

Composite	Additives	Method	T, °C	Conditions	Structure	R *, Ω·cm	Ref.
SiC–50 mol%-AlN	5 mol% Y_2O_3	PL *	2000	Ar, 8 h	SS+SiC	10^{18}	[29]
SiC–50 mol%-AlN	5 mol% Y_2O_3	PL *	2000	N_2, 8 h	SS+SiC	10^{17}	[29]
SiC–35 vol.%-AlN	-	HP *	1950	Ar, 2 h, 40 MPa	SS+SiC	1.1×10^{10}	[37]
AlN–SiC	Y_2O_3	PL *	2000	N_2	AlN+SiC	10^5–10^9 **	[5]
SiC–50 mol%-AlN	0.2 wt.% B 1.0 wt.% C	HP *	2100	1 h, 35 MPa	SS	4.0×10^6	[38]
SiC–50 mol%-AlN	-	SPS *	1900–2100	Ar, 30 min, 50 MPa	SS+SiC	10^3 –10^5	[21]
35 vol.%-SiC–AlN	4 wt.% Al_2O_3 + 2 wt.% Y_2O_3	HP	1900	N_2, 1.5 h, 25 MPa	AlN+SS+SiC	~10^4	[3]
SiC–30 wt.%-AlN	5 wt.% Al_2O_3–Y_2O_3	PL *	2080	Vacuum, 2 h	AlN+SS+SiC	1.1×10^1	[32]
SiC–50 mol%-AlN	-	PL *	2000	Ar, 1 h	SS	3.3×10^1	[36]

*: T—Sintering temperature, R—Resistivity; HP—Hot Press; SPS—Spark Plasma Sintering; PL—Pressureless.
**: For different SiC grain sizes from 40 nm to 5 μm.

4. Conclusions

In this paper, the dependence of the microstructure and properties on spark plasma sintering modes of an AlN-35 β-SiC (wt.%) composite is investigated. The influence of the heating rate on the phase composition and microstructure of the obtained composites has been established. It was found that the use of a heating rate of 100 °C/min during the sintering process of the AlN-35 β-SiC (wt.%) composite leads to the formation of a solid solution $(AlN)_x$–$(SiC)_{x-1}$ at a pressure of 50 MPa, a sintering temperature of 1900 °C, and

a dwell of 5 min. In addition, it was observed that, at a heating rate of 50 °C/min and a pressure of 25 MPa, yttrium oxide used as a sintering additive prevents the diffusion of SiC into AlN. This prevents the formation of a solid solution $(AlN)_x$–$(SiC)_{x-1}$ and helps preserve SiC grains, which act as the main absorbing phase, in the obtained composites. Furthermore, it is shown that the use of sintering additives and SPS technology allows for the obtaining of samples with a density of 3.26 g/cm^3, which coincides with the theoretical value of the compound.

The dielectric characteristics and absorbing properties of the synthesized materials are determined. It has been found that, with a decrease in the composite sample thickness, the reflection, transmission, and absorption coefficients shift towards high frequencies, which allows these properties to be regulated depending on the sample thickness. In addition, it is shown that composites containing solid solutions and silicon carbide grains in their structures have the best absorbing properties. On the other hand, the material containing only solid solutions is a promising material that can be used as microwave filters.

Author Contributions: Conceptualization, T.N.S. and A.S.; data curation, L.A.; formal analysis, A.D.S., T.N.S. and N.W.S.P.; funding acquisition, N.W.S.P.; methodology, T.N.S., V.E.B. and A.D.S.; project administration, N.W.S.P.; resources, L.A. and A.S.; software, V.E.B. and Y.P.; supervision, T.N.S.; validation, A.D.S. and Y.P.; visualization, V.E.B.; writing—original draft, N.W.S.P. and T.N.S. All authors have read and agreed to the published version of the manuscript.

Funding: The work of Nestor Washington Solis Pinargote and Anton Smirnov was supported by the Russian Science Foundation (Grant Agreement No. 23-19-00413, https://rscf.ru/project/23-19-00413/) accessed on 28 November 2025.

Data Availability Statement: The original contributions presented in this study are included in the article. Further inquiries can be directed to the corresponding authors.

Acknowledgments: This study was carried out on the equipment of the Center of Collective Use "State Engineering Center" of the MSUT "STANKIN".

Conflicts of Interest: The authors declare no conflicts of interest.

References

1. Белова, Г.С.; Титова, Ю.В.; Самборук, А.Р. Получение керамической нитридно-карбидной нанопорошковой композиции AlN-SiC по азидной технологии СВС. *Современные Материалы Техника и Технологии* **2020**, *3*, 17–26.
2. Xiang-Yu, Z.; Shou-Hong, T.; Wei-Wei, X.; Shao-Ming, D.; Zheng-Ren, H.; Ye, D.; Pei-Heng, W.; Dong-Liang, J. Preparation and dielectric properties of SiC-AlN solid solutions. *Key Eng. Mater.* **2005**, *280–283*, 127–130. [CrossRef]
3. Fang, X.; Jiang, S.; Pan, L.; Yin, S.; Qiu, T.; Yang, J.; Li, X. β-SiC/AlN microwave attenuating composite ceramics with excellent and tunable microwave absorption properties. *J. Eur. Ceram. Soc.* **2021**, *41*, 6385–6392. [CrossRef]
4. Serbenyuk, T.B.; Prikhna, T.O.; Sverdun, V.B.; Chasnyk, V.I.; Karpets, M.V.; Basyuk, T.V. The effect of size of the SiC inclusions in the AlN-SiC composite structure on the electrophysical properties. *J. Superhard Mater.* **2016**, *38*, 241–250. [CrossRef]
5. Lu, Y.; Zang, X.; Du, B. Investigation of the effect of the SiC particle size on the properties of the AlN–SiC composite ceramic. *Mater. Chem. Phys.* **2021**, *261*, 124222. [CrossRef]
6. Gu, J.; Sang, L.; Pan, B.; Feng, Y.; Yang, J.; Li, X. Thermal Conductivity and High-Frequency Dielectric Properties of Pressureless Sintered SiC-AlN Multiphase Ceramics. *Materials* **2018**, *11*, 969. [CrossRef]
7. Prikhna, T.O.; Serbenyuk, T.B.; Sverdun, V.B.; Chasnyk, V.I.; Karpets, M.V.; Basyuk, T.V.; Dellikh, J. Formation regulations of structures of AlN-SiC-based ceramic materials. *J. Superhard Mater.* **2015**, *37*, 293–299. [CrossRef]
8. Tsyganenko, V.S.; Lytyuga, N.V.; Dubovik, T.V.; Kozina, G.K.; Rogozinskaya, A.A.; Panashenko, V.M. Effect of the Al_2O_3 additives on the properties of the ceramic based on aluminum nitride. *Powder Metall.* **2006**, *9*, 45–49. [CrossRef]
9. Nepochatov, Y.; Zemnitskaya, A.; Mul, P. The development of ceramics based on aluminum nitride for products of electronic engineering. *Mod. Electron.* **2011**, *9*, 14–16.
10. Kim, Y.-W.; Mitomo, M.; Nishiruma, T. Heat-resistant silicon carbide with aluminum nitride and erbium oxide. *J. Am. Ceram. Soc.* **2001**, *84*, 2060–2064. [CrossRef]

11. Gao, P.; Jia, C.C.; Cao, W.B. Dielectric properties of spark plasma sintered AlN/SiC composite ceramics. *Int. J. Miner. Metall. Mater.* **2014**, *21*, 589–594. [CrossRef]
12. Shirouzu, K.; Nonaka, Y.; Hotta, M.; Enomoto, N.; Hojo, J. Synthesis and microstructural evaluation of SiC-AlN composites. *Key Eng. Mater.* **2007**, *352*, 193–196. [CrossRef]
13. Сафаралиев, Г.К.; Шабанов, Ш.Ш.; Садыков, С.А.; Агаларов, А.Ш.; Билалов, Б.А. Диэлектрическая релаксация в поликристаллических твердых растворах SiC–AlN. *Вестник Дагестанского Государственного Университета* **2011**, *6*, 27–30.
14. Guo, X.; Feng, Y.; Lin, X.; Liu, Y.; Gong, H.; Zhang, Y. The dielectric and microwave absorption properties of polymer-derived SiCN ceramics. *J. Eur. Ceram. Soc.* **2018**, *38*, 1327–1333. [CrossRef]
15. Li, P.W.; Wang, C.B.; Liu, H.X.; Shen, Q.; Zhang, L.M. Structural, thermal and dielectric properties of AlN–SiC composites fabricated by plasma activated sintering. *Adv. Appl. Ceram.* **2019**, *118*, 313–320. [CrossRef]
16. Zangvil, A.; Ruh, R. Phase Relationships in the Silicon Carbide—Aluminum Nitride System. *J. Am. Ceram. Soc.* **1988**, *71*, 884–890. [CrossRef]
17. Solís Pinargote, N.W.; Pristinskiy, Y.; Meleshkin, Y.; Kurmysheva, A.Y.; Mozhaev, A.; Lavreshin, N.; Smirnov, A. Prediction of Physical and Mechanical Properties of Al_2O_3–TiB_2–TiC Composites Using Design of Mixture Experiments. *Ceramics* **2024**, *7*, 1639–1657. [CrossRef]
18. Grigoriev, S.N.; Pristinskiy, Y.; Soe, T.N.; Malakhinsky, A.; Mosyanov, M.; Podrabinnik, P.; Smirnov, A.; Solís Pinargote, N.W. Processing and Characterization of Spark Plasma Sintered SiC-TiB_2-TiC Powders. *Materials* **2022**, *15*, 1946. [CrossRef]
19. Smirnov, A.; Pristinskiy, Y.; Pinargote, N.W.S.; Meleshkin, Y.; Podrabinnik, P.; Volosova, M.; Grigoriev, S. Mechanical Performance and Tribological Behavior of WC-ZrO_2 Composites with Different Content of Graphene Oxide Fabricated by Spark Plasma, Sintering. *Sci* **2024**, *6*, 82. [CrossRef]
20. Zhang, X.Y.; Tan, S.H.; Zhang, J.X.; Jiang, D.L.; Hu, B.; Gao, C. Lossy AlN–SiC composites fabricated by spark plasma sintering. *J. Mater. Res.* **2004**, *19*, 2759–2764. [CrossRef]
21. Hojo, J.; Nonaka, Y.; Kamada, K.; Enomoto, N.; Hotta, M.; Shirouzu, K. Fabrication and electrical property of SiC-AlN composites. *Mater. Sci. Forum* **2007**, *561–565*, 607–611. [CrossRef]
22. Hojo, J.; Matsuura, H.; Hotta, M. Nano-Grained Microstructure Design of Silicon Carbide Ceramics by SPS Process. *Key Eng. Mater.* **2009**, *403*, 177–178. [CrossRef]
23. Kobayashi, R.; Tatami, J.; Wei Chen, I.; Wakihara, T.; Komeya, K.; Meguro, T. High temperature mechanical properties of dense AlN–SiC ceramics fabricated by spark plasma sintering without sintering additives. *J. Amer. Ceram. Soc.* **2011**, *94*, 4150–4153. [CrossRef]
24. Kobayashi, R.; Tatami, J.; Wakihara, T.; Komeya, K.; Meguro, T.; Goto, T.; Tu, R. Use of Post–heat Treatment to Obtain a 2H Solid Solution in Spark Plasma Sintering--Processed AlN–SiC Mixtures. *J. Amer. Ceram. Soc.* **2008**, *91*, 1548–1552. [CrossRef]
25. Nicolson, A.M.; Ross, G.F. Measurement of the intrinsic properties of materials by time-domain techniques. *IEEE Trans. Instrum. Meas.* **1970**, *IM-19*, 377–382. [CrossRef]
26. Parkhomenko, M.P.; Kalenov, D.S.; Eremin, I.S.; Fedoseev, N.A.; Kolesnikova, V.M.; Dyakonova, O.A. Improving the accuracy in measuring the complex dielectric and magnetic permeabilities in the microwave range using the waveguide method. *J. Commun. Technol. Electron.* **2020**, *65*, 894–898. [CrossRef]
27. Somasundaram, M.; Uttamchand, N.K.; Annamalai, A.R.; Jen, C.-P. Insights on Spark Plasma Sintering of Magnesium Composites: A Review. *Nanomaterials* **2022**, *12*, 2178. [CrossRef]
28. Olevsky, E.A.; Kandukuri, S.; Froyen, L. Consolidation enhancement in spark-plasma sintering: Impact of high heating rates. *J. Appl. Phys.* **2007**, *102*, 114913. [CrossRef]
29. Kultayeva, S.; Kim, Y.-W. Mechanical, thermal, and electrical properties of pressureless sintered SiC–AlN ceramics. *Ceram. Int.* **2020**, *46*, 19264–19273. [CrossRef]
30. Lee, J.K.; Tanaka, H.; Kim, H. Formation of solid solutions between SiC and AlN during liquid-phase sintering. *Mater. Lett.* **1996**, *29*, 1–6. [CrossRef]
31. Hotta, M.; Hojo, J. Inhibition of grain growth in liquid-phase sintered SiC ceramics by AlN additive and spark plasma sintering. *J. Eur. Ceram. Soc.* **2010**, *30*, 2117–2122. [CrossRef]
32. Besisa, D.H.A.; Ewais, E.M.M.; Shalaby, E.A.M.; Usenko, A.; Kuznetsov, D.V. Thermoelectric properties and thermal stress simulation of pressureless sintered SiC/AlN ceramic composites at high temperatures. *Sol. Energy Mater. Sol. Cells* **2018**, *182*, 302–313. [CrossRef]
33. Pan, Y.B.; Qiu, J.H.; Morita, M.; Tan, S.H.; Jiang, D. The mechanical properties and microstructure of SiC–AlN particulate composite. *J. Mater. Sci.* **1998**, *33*, 1233–1237. [CrossRef]
34. Yakubu, A.; Abbas, Z.; Hashim, M. Effect of Material Thickness on Attenuation (dB) of PTFE Using Finite Element Method at X-Band Frequency. *Adv. Mater. Sci. Eng.* **2014**, *2014*, 965912. [CrossRef]

35. Deep, S.; Sharma, V. Effects of Microstructures, Heterogeneity, and Imperfectness on Propagation of SH-Waves in a Fiber-Reinforced Layer Sandwiched Between Two Microstructural Half-Spaces. *Iran J. Sci. Technol. Trans. Mech. Eng.* **2023**, *47*, 1161–1176. [CrossRef]
36. Kobayashi, R.; Tatami, J.; Wakihara, T.; Meguro, T.; Komeya, K. Temperature dependence of the electrical properties and Seebeck coefficient of AlN–SiC ceramics. *J. Am. Ceram. Soc.* **2006**, *89*, 1295–1299. [CrossRef]
37. Kim, K.J.; Kim, Y.W.; Lim, K.Y.; Nishimura, T.; Narimatsu, E. Electrical and thermal properties of SiC–AlN ceramics without sintering additives. *J. Eur. Ceram. Soc.* **2015**, *35*, 2715–2721. [CrossRef]
38. Ou, R.; Qin, H.; Gerhardt, R.A.; Ruh, R. Electrical properties of SiC-AlN composite. *Ceram. Eng. Sci. Proc.* **2003**, *24*, 349–354. [CrossRef]

Disclaimer/Publisher's Note: The statements, opinions and data contained in all publications are solely those of the individual author(s) and contributor(s) and not of MDPI and/or the editor(s). MDPI and/or the editor(s) disclaim responsibility for any injury to people or property resulting from any ideas, methods, instructions or products referred to in the content.